Indian Journal of Pure & Applied Physics
Vol. 56, December 2018, pp. 931-940

Newtonian heating and convective boundary condition on MHD stagnation point flow past a stretching sheet with viscous dissipation and Joule heating

Santosh Chaudhary*, KM Kanika & Mohan Kumar Choudhary

Department of Mathematics, Malaviya National Institute of Technology, Jaipur 302 017, India

Received 8 September 2017; accepted 10 July 2018

An analysis has been presented to study the effects of viscous dissipation and Joule heating on two-dimensional steady stagnation-point flow of an incompressible viscous electrically conducting fluid over a stretching plate with Newtonian heating and convective boundary condition in the presence of uniform transverse magnetic field. Similarity variables reduce the governing boundary layer partial differential equations to a set of non-linear ordinary differential equations and solved numerically using the Galerkin finite element method. Effects of various parameters such as stretching parameter, magnetic parameter, conjugate parameter, Prandtl number and Eckert number for velocity and temperature distributions have been discussed in detail through graphical representation. Moreover, numerical results of local skin-friction coefficient and local Nusselt number for different values of controlling parameters have been shown in tabular form and analyzed. Numerical values have been validated by comparing the present results with previously published works.

Keywords: Newtonian heating, Convective boundary condition, MHD flow, Stagnation point, Stretching sheet, Viscous dissipation, Joule heating

1 Introduction

Magnetohydrodynamic (MHD) is the study of the interaction of conducting fluids with electromagnetic phenomena. It has aroused a great deal of research interest due to wide applications to problems of engineering and industrial nature, such as MHD power generators, plasma studies, boundary layer control in aerodynamics, crystal growth, MHD flow meters, MHD pumps and petroleum industries. Rossow[1] was the first to study the magnetohydrodynamic effects of the boundary layer on a semi-infinite plate in the presence of uniform transverse magnetic field. Further, Andersson[2] investigated the MHD flow of viscoelastic fluid past a stretching sheet in the presence of a uniform transverse magnetic field. Several researchers such as Ariel[3], Attia[4], Duwairi and Duwairi[5], Xu and Liao[6], Chen[7], Fang and Zhang[8], Jat and Chaudhary[9], Guedda and Ouahsine[10], Chaudhary and Kumar[11] and Dogonchi *et al.*[12] studied the problem of MHD flow in various aspects.

Stagnation point flow interprets the fluid motion near the stagnation region which exists on solid bodies when the fluid moves towards it. This region encounters the highest pressure, the highest rate of heat transfer and mass deposition. It is a topic of great significance in fluid mechanics due to its wide applications in almost all flow fields of science and engineering. Examples of such technological processes are heat exchangers placed in a low-velocity environment, many hydrodynamic processes and solar central receivers exposed to wind currents. Pursuing the pioneering study by Hiemenz[13] who considered the steady two dimensional boundary layer flow in the neighbourhood of a stagnation point on an infinite wall, many researchers like Homann[14], Chiam[15], Lok *et al.*[16], Reza and Gupta[17] and Nadeem *et al.*[18] have analyzed the problem of stagnation point flow in numerous ways to include various physical effects. A representative sample of the recent literature on this topic is provided by Ja'fari and Rahimi[19] and Chaudhary and Choudhary[20].

Stretching surface is important in number of industrial manufacturing processes that build both metal and polymer sheets in a quiescent or moving fluid. Its applications are also seen in extrusion, metal spinning, hot rolling, wire drawing, glass-fibre, paper production and condensation process of metallic plate in a cooling bath. An extensive variation of problems dealing with heat and fluid flow over a stretching sheet have been studied with both Newtonian and non-Newtonian fluids with the formation of imposed electric and magnetic fields, power law variation of

*Corresponding author (E-mail: d11.santosh@yahoo.com)

the stretching velocity, and different thermal boundary conditions. The boundary layer flow towards a stretching sheet under different conditions is given by Crane[21], Siddappa and Abel[22], Liao[23] and Makinde and Sibanda[24]. However, some most recent works of distinguished researchers mentioned in the studies Pal[25] and Chaudhary *et al.*[26] describing the flow over stretching sheet with heat transfer.

Viscous dissipation in the natural convection flow is peculiarized by the Eckert number. Its role is well appreciated when the flow field is of extreme size or in high gravitational field. The repercussion of Joule heating on magnetic field is a significantly apparent physical phenomenon in fluid mechanics which may be seen in diverse industrial processes for instant chemical and food processing, oil exploration and bioengineering. Joule heating, in electronics and physics, denotes the increment in temperature of the conductor as an after-effect of resistance to the electrical current flowing through it. The influence of Joule heating is essentially represented by the product of the Eckert number and the magnetic parameter. The influence and importance of viscous dissipation effects have been examined by Nield[27] and Roy and Murthy[28]. The combine effects of viscous dissipation and Joule heating over immobile or mobile surface corresponding to the various boundary conditions are scarcely bound in the literature such as El- Amin[29], Abo-Eldahab and El Aziz[30], Jat and Chaudhary[31], Palani and Kim[32], Chakraborty *et al.*[33] and Hayat *et al.*[34].

Thermal convection may occur in the presence of Newtonian heating due to exchange of heat between the surface and the ambient fluid. Application of Newtonian heating can be found in solar power collectors, cooling mechanism for nuclear reactors, heat exchangers where conduction influences the convection, and other processes. Merkin[35], Lesnic *et al.*[36] and Salleh *et al.*[37], presented the boundary layer flow with Newtonian heating under different situations. Moreover, convective heat transfer plays a key role in procedures in which high temperature are involved, such as nuclear plants, gas turbines, storage of thermal energy, electronic devices, computer power supply and also in engine cooling system like heatsink in a car radiator. The convective boundary conditions are more practical in industrial and engineering processes, including transpiration cooling process, material drying and many more. Recently, Aydin and Kaya[38], Yao *et al.*[39], Nandy and Mahapatra[40] and Ibrahim and Haq[41] presented an excellent review of heat transfer problems with a convective boundary condition and related applications.

Main objective of the present study is to extend the research of Mohamed *et al.*[42] with viscous dissipation and Joule heating effects on an electrically conducting fluid in the presence of uniform transverse magnetic field.

2 Mathematical Model

Two-dimensional, steady, laminar, incompressible, electrically conducting stagnation point flow over a stretching surface of constant temperature T_w is considered. Rectangular coordinates (x, y) are used, in which the $x-$ and $y-$axes are taken as the coordinates parallel to the plate and normal to it, respectively. Their origin is taken to be coincident with the stagnation point, and the fluid occupied along $y > 0$ as shown in Fig. 1. A uniform magnetic field of strength B_0 is assumed to be applied normal to the stretching plate. The induced magnetic field comes out to be negligible if the magnetic Reynolds number is taken very small. It is also surmised that the external velocity $u_e(x) = ax$ and the stretching velocity $u_w(x) = bx$, where a and b are positive constants and x is the coordinate measured along the stretching surface. The ambient fluid temperature T_∞ is constant. Under the boundary layer approximation and the presumptions, the basic equations are:

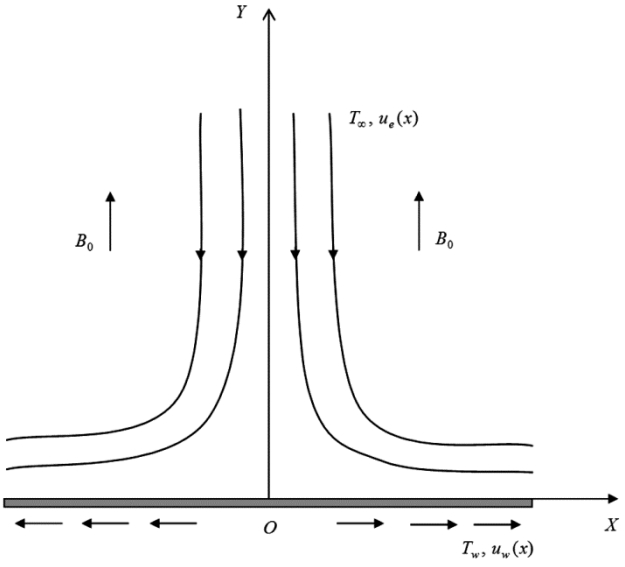

Fig. 1 – Flow geometry and coordinate system.

$$\frac{\partial u}{\partial x}+\frac{\partial v}{\partial y}=0 \qquad \ldots(1)$$

$$u\frac{\partial u}{\partial x}+v\frac{\partial u}{\partial y}=u_e\frac{du_e}{dx}+\upsilon\frac{\partial^2 u}{\partial y^2}-\frac{\sigma_e {B_0}^2}{\rho}(u-u_e) \qquad \ldots(2)$$

$$u\frac{\partial T}{\partial x}+v\frac{\partial T}{\partial y}=\alpha\frac{\partial^2 T}{\partial y^2}+\frac{\mu}{\rho C_p}\left(\frac{\partial u}{\partial y}\right)^2+\frac{\sigma_e {B_0}^2}{\rho C_p}(u-u_e)^2 \qquad \ldots(3)$$

with the appropriate boundary conditions

$$y=0:\ u=u_w(x),\ v=0,\ \frac{\partial T}{\partial y}=-h_w T\ \text{(NH)},\ -\kappa\frac{\partial T}{\partial y}=h_w(T_w-T)\ \text{(CBC)}$$
$$y\to\infty:\ u\to u_e(x),\ T\to T_\infty \qquad \ldots(4)$$

where u and v are the velocity components in the x and y directions, respectively. $\upsilon=\frac{\mu}{\rho}$ is the kinematic viscosity, μ is the coefficient of viscosity, ρ is the fluid density, σ_e is the electrical conductivity, T is temperature of the fluid, α is the thermal diffusivity, C_p is the specific heat at constant pressure, h_w is the heat transfer coefficient and κ is the thermal conductivity.

3 Similarity Transformation

Introducing the following non-dimensional similarity variables (Mohamed *et al.*[42]):

$$\psi(x,y)=(\upsilon u_e x)^{1/2} f(\eta) \qquad \ldots(5)$$

$$\eta=\left(\frac{u_e}{\upsilon x}\right)^{1/2} y \qquad \ldots(6)$$

$$T=T_\infty[1+\theta(\eta)]\ \text{(NH)},\quad T=T_\infty+(T_w-T_\infty)\theta(\eta)\ \text{(CBC)} \qquad \ldots(7)$$

where $\psi(x,y)$ is the stream function, defined as $u=\frac{\partial\psi}{\partial y}$ and $v=-\frac{\partial\psi}{\partial x}$, which identically satisfies the continuity Eq. (1) , $f(\eta)$ is the dimensionless stream function, η is the similarity variable, y is the coordinate measured along normal to the stretching sheet and $\theta(\eta)$ is the dimensionless temperature. The momentum and energy Eqs (2) and (3) with the boundary conditions Eq. (4), reduce to the following nonlinear differential equations:

$$f'''+ff''-f'^2-M(f'-1)+1=0 \qquad \ldots(8)$$

$$\frac{1}{\Pr}\theta''+f\theta'+Ec[f''^2+M(f'-1)^2]=0 \qquad \ldots(9)$$

with the corresponding boundary conditions

$$\eta=0:\ f=0,\ f'=\varepsilon,\ \theta'=-\gamma(1+\theta)\ \text{(NH)},\ \theta'=-\gamma(1-\theta)\ \text{(CBC)}$$
$$\eta\to\infty:\ f'\to 1,\ \theta\to 0 \qquad \ldots(10)$$

where primes denote differentiation with respect to η, $M=\frac{\sigma_e {B_0}^2}{\rho a}$ is the magnetic parameter, $\Pr=\frac{\upsilon}{\alpha}$ is the Prandtl number, $Ec=\frac{{u_e}^2}{C_p T_\infty}$ (NH) or $Ec=\frac{{u_e}^2}{C_p(T_w-T_\infty)}$ (CBC) is the Eckert number, $\varepsilon=\frac{b}{a}$ is the stretching parameter and $\gamma=\left(\frac{\upsilon}{a}\right)^{1/2}h_w$ (NH) or $\gamma=\left(\frac{\upsilon}{a}\right)^{1/2}\frac{h_w}{\kappa}\gamma$ (CBC) is the conjugate parameter for the convective boundary condition.

4 Local Skin Friction and Local Nusselt Number

The physical quantities of interest are the local skin friction coefficient C_f and the local Nusselt number Nu_x, which are defined as:

$$C_f=\frac{\tau_w}{\frac{\rho {u_e}^2}{2}} \qquad \ldots(11)$$

$$Nu_x=\frac{x q_w}{\kappa(T_w-T_\infty)} \qquad \ldots(12)$$

where $\tau_w=\mu\left(\frac{\partial u}{\partial y}\right)_{y=0}$ is the surface shear stress and $q_w=-\kappa\left(\frac{\partial T}{\partial y}\right)_{y=0}$ is the surface heat flux.

Using the similarity transformations Eqs (5) to (7), the Eqs (11) and (12) can be obtained as follows:

$$C_f=\frac{2}{(\mathrm{Re}_x)^{1/2}}f''(0) \qquad \ldots(13)$$

$$Nu_x = -\frac{(\mathrm{Re}_x)^{1/2}}{\theta(0)}\theta'(0)\,(\mathrm{NH}),\ Nu_x = -(\mathrm{Re}_x)^{1/2}\theta'(0)\,(\mathrm{CBC}) \quad \ldots(14)$$

where $\mathrm{Re}_x = \dfrac{u_e x}{\upsilon}$ is the local Reynolds number.

5 Method of Solution

Galerkin finite element method is employed to solve the system of non-linear ordinary differential Eqs (8) and (9) along with the boundary conditions Eq. (10). For the computational directions, suitable finite values for the far field boundary conditions as $\eta \to \infty = 6$ is assumed. The whole domain is divided into a set of 1000 linear line elements of equal size $\Delta\eta = 0.006$, each element having two nodes.

Introducing

$$f' = h \quad \ldots (15)$$

then the system of Eqs (8) and (9) are reduced to the following forms:

$$h'' + fh' - h^2 - M(h-1) + 1 = 0 \quad \ldots (16)$$

$$\frac{1}{\mathrm{Pr}}\theta'' + f\theta' + Ec\left[h'^2 + M(h-1)^2\right] = 0 \quad \ldots (17)$$

with the converted boundary conditions

$$\eta = 0:\ f = 0,\ h = \varepsilon,\ \theta' = -\gamma(1+\theta)\ (\mathrm{NH}),\ \theta' = -\gamma(1-\theta)\ (\mathrm{CBC})$$
$$\eta = 6:\ h \to 1,\ \theta \to 0 \quad \ldots (18)$$

The variational form of Eqs (15) to (17) over an individual line element (η_e, η_{e+1}) is written as:

$$\int_{\eta_e}^{\eta_{e+1}} w_1 (f' - h)\, d\eta = 0 \quad \ldots (19)$$

$$\int_{\eta_e}^{\eta_{e+1}} w_2 \left[h'' + fh' - h^2 - M(h-1) + 1\right] d\eta = 0 \quad \ldots (20)$$

$$\int_{\eta_e}^{\eta_{e+1}} w_3 \left\{\frac{1}{\mathrm{Pr}}\theta'' + f\theta' + Ec\left[h'^2 + M(h-1)^2\right]\right\} d\eta = 0 \quad \ldots (21)$$

where w_1, w_2 and w_3 are weight functions corresponding to functions f, h and θ, respectively. The finite element approximations of the functions f, h and θ are considered as $f = \sum_{j=1}^{2} f_j \varphi_j$, $h = \sum_{j=1}^{2} h_j \varphi_j$, $\theta = \sum_{j=1}^{2} \theta_j \varphi_j$ with $w_1 = w_2 = w_3 = \varphi_i$, $(i = 1, 2)$.

Where φ_i are the shape functions for a typical linear element (η_e, η_{e+1}) and are taken as:

$$\varphi_1^{(e)} = \frac{\eta_{e+1} - \eta}{\eta_{e+1} - \eta_e},\ \varphi_2^{(e)} = \frac{\eta - \eta_e}{\eta_{e+1} - \eta_e},\ \eta_e \le \eta \le \eta_{e+1}$$

Hence, the finite element model of the Eqs (19) to (21) is given by:

$$\begin{bmatrix} [K^{11}] & [K^{12}] & [K^{13}] \\ [K^{21}] & [K^{22}] & [K^{23}] \\ [K^{31}] & [K^{32}] & [K^{33}] \end{bmatrix} \begin{bmatrix} \{f\} \\ \{h\} \\ \{\theta\} \end{bmatrix} = \begin{bmatrix} \{b^1\} \\ \{b^2\} \\ \{b^3\} \end{bmatrix} \quad \ldots (22)$$

where $\left[K^{mn}\right]$ and $\left[b^m\right]$ $(m = 1, 2$ and $n = 1, 2)$ are defined as

$$K_{ij}^{11} = \int_{\eta_e}^{\eta_{e+1}} \varphi_i \frac{d\varphi_j}{d\eta} d\eta,\ K_{ij}^{12} = -\int_{\eta_e}^{\eta_{e+1}} \varphi_i \varphi_j d\eta,\ K_{ij}^{13} = 0$$

$$K_{ij}^{21} = 0,\ K_{ij}^{22} = \int_{\eta_e}^{\eta_{e+1}} \left[-\frac{d\varphi_i}{d\eta}\frac{d\varphi_j}{d\eta} + \bar{f}\varphi_i \frac{d\varphi_j}{d\eta} - (\bar{h} + M)\varphi_i \varphi_j\right] d\eta,\ K_{ij}^{23} = 0$$

$$K_{ij}^{31} = 0,\ K_{ij}^{32} = Ec\int_{\eta_e}^{\eta_{e+1}} \left[\bar{h}'\varphi_i \frac{d\varphi_j}{d\eta} + M(\bar{h} - 2)\varphi_i \varphi_j\right] d\eta,\ K_{ij}^{33} = \int_{\eta_e}^{\eta_{e+1}} \left[-\frac{1}{\mathrm{Pr}}\frac{d\varphi_i}{d\eta}\frac{d\varphi_j}{d\eta} + \bar{f}\varphi_i \frac{d\varphi_j}{d\eta}\right] d\eta$$

and

$$b_i^1 = 0,\ b_i^2 = -\left(\varphi_i \frac{dh}{d\eta}\right)_{\eta_e}^{\eta_{e+1}} - (M+1)\int_{\eta_e}^{\eta_{e+1}} \varphi_i d\eta,$$

$$b_i^3 = -\frac{1}{\mathrm{Pr}}\left(\varphi_i \frac{d\theta}{d\eta}\right)_{\eta_e}^{\eta_{e+1}} - MEc\int_{\eta_e}^{\eta_{e+1}} \varphi_i d\eta$$

with

$$\bar{f} = \sum_{i=1}^{2} \bar{f}_i \varphi_i,\ \bar{h} = \sum_{i=1}^{2} \bar{h}_i \varphi_i,\ \bar{h}' = \sum_{i=1}^{2} \bar{h}_i' \varphi_i,\ \bar{\theta} = \sum_{i=1}^{2} \bar{\theta}_i \varphi_i.$$

The entire flow domain is split into the 1000 equal size linear elements and three functions are to be computed at every node. Therefore, after assemble of all element equations, a matrix of order 3003×3003 is obtained. An iterative process must be utilized for the solution of the constructed linear system. After employing the boundary conditions only the system of 2998 equations remain, which is determined by the Newton-Raphson method while maintaining an accuracy of 10^{-7}.

6 Validation of the Numerical Method

To ensure the consistency of the method and reliability of the present analysis, comparisons of the local skin friction coefficient $f''(0)$ for various values of the stretching parameter ε in the absence of the magnetic parameter M with available results of Wang[43], Yacob and Ishak[44] and Mohamed *et al.*[42] are recorded in Table 1. The numerical results obtained by the Galerkin finite element method are in excellent agreement with the earlier published research works, concluding the method to be valid.

7 Results and Discussion

In this section the effects of different pertinent physical parameters namely the stretching parameter ε, the magnetic parameter M, the conjugate parameter γ, the Prandtl number Pr and the Eckert number Ec on the distributions of velocity $f'(\eta)$ and temperature $\theta(\eta)$ are described through graphs. Moreover, the computational results of the shear stress $f''(0)$ and the heat transfer rate $\theta'(0)$ regarding the above mentioned various controlling parameters are tabulated.

Figure 2 depicts the influence of the stretching parameter ε on the velocity $f'(\eta)$ profiles while in Figs 3 and 4 on temperature $\theta(\eta)$ profiles for the NH and CBC cases, respectively, keeping other controlling parameters constant. It is clear from these figures that the velocity increases with the increase in the stretching parameter ε. Further, the flow has an inverted boundary layer structure when $\varepsilon > 1$. Moreover the temperature is decreased with the increase of the stretching parameter ε while in the case of NH, the opposite is true for $\eta > 2$. Physically, when the free stream velocity is greater than stretching velocity, i.e., the ratio of free stream velocity to stretching velocity is greater than one, the retarding force diminishes and the flow velocity increases while thermal boundary layer thickness reduces.

The effects of the magnetic parameter M on the fluid flow $f'(\eta)$ and the temperature $\theta(\eta)$ distribution for all cases are shown in Figs 5 and 6 to 7, respectively, while the other pertinent physical parameters are constant. These figures show that an increase in the value of the magnetic parameter M leads to an increase in the fluid velocity. Moreover it is evident that the dimensionless temperature for the case NH is reduced with the increasing amount of the value of the magnetic parameter M but the opposite phenomenon occurs for $\eta > 1.5$. It is also noticeable that the reverse behaviors as compared to NH case are observed for the case of CBC. From a physical point of view, the Lorentz force increases with the rise in magnetic parameter leading to development of resistance to fluid flow which inturn generates more heat resulting in enhancement of temperature field.

Table 1 – comparison for the values of $f''(0)$ with the previously published results when $M = 0.0$.

ε	$f''(0)$			
	Wang[43]	Yacob and Ishak[44]	Mohamed *et al.*[42]	Present results
0.0	1.232588	1.232588	1.2325877	1.232588
0.1	1.14656	-	-	1.146561
0.2	1.05113	-	-	1.051130
0.5	0.71330	0.713295	0.7132949	0.713295
1.0	0.00000	0.000000	0.0000000	0.000000
2.0	-1.88731	-1.887307	-1.8873066	-1.887304
5.0	-10.26475	-	-	-10.264746

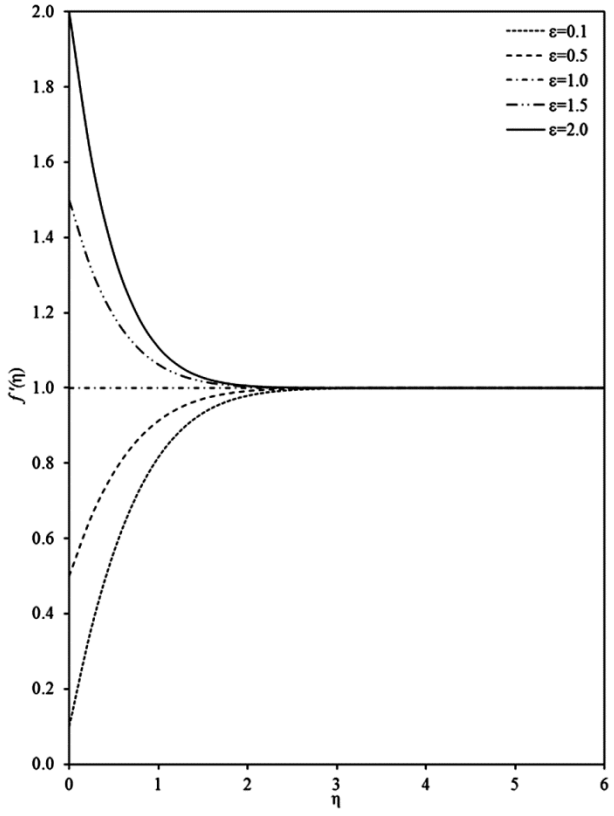

Fig. 2 – Velocity profiles for several values of ε with $M = 0.1$.

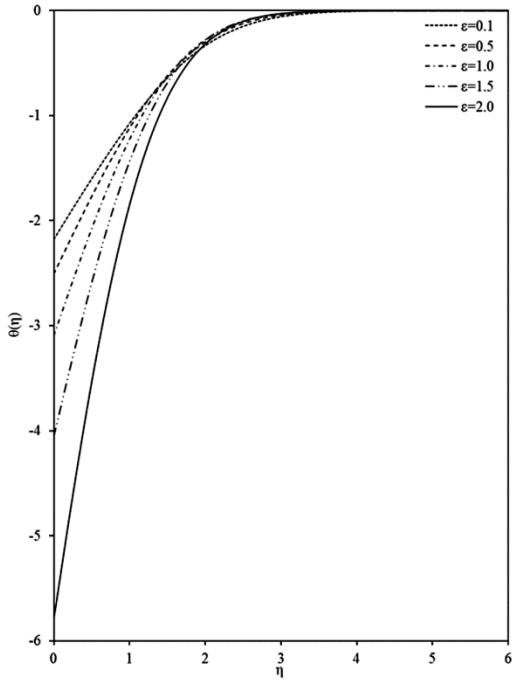

Fig. 3 – Temperature profiles of the NH case for several values of ε with $M = 0.1$, $\gamma = 1.0$, $\Pr = 0.72$ and $Ec = 0.1$.

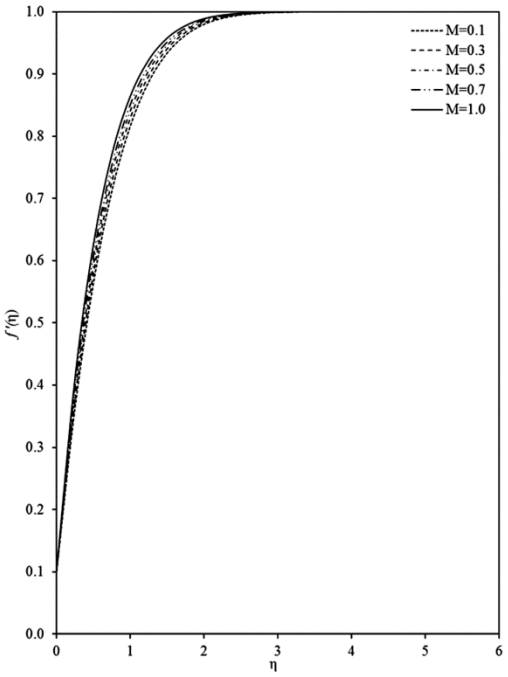

Fig. 5 – Velocity profiles for several values of M with $\varepsilon = 0.1$.

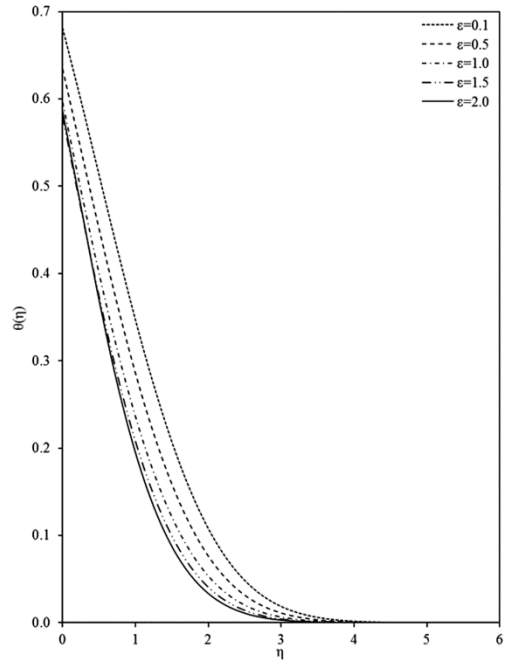

Fig. 4 – Temperature profiles of the CBC case for several values of ε with $M = 0.1$, $\gamma = 1.0$, $\Pr = 0.72$ and $Ec = 0.1$.

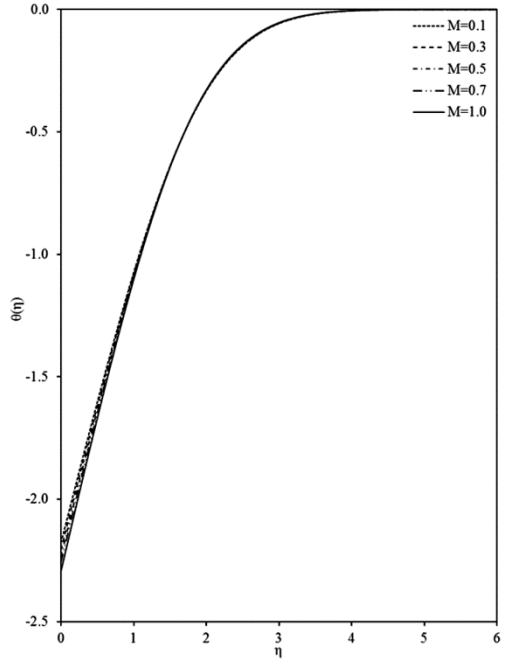

Fig. 6 – Temperature profiles of the NH case for several values of M with $\varepsilon = 0.1$, $\gamma = 1.0$, $\Pr = 0.72$ and $Ec = 0.1$.

Figures 8 and 9 illustrate the influences of the conjugate parameter γ on the temperature $\theta(\eta)$ profiles for the cases NH and CBC, respectively, where the other parameters are kept constant. In the case of NH, it is observed that the temperature of a flow field is an increasing function of the conjugate parameter γ for $\gamma < 1$, same behavior is noted in opposite direction for $\gamma \geq 1$. Whereas, for the case of

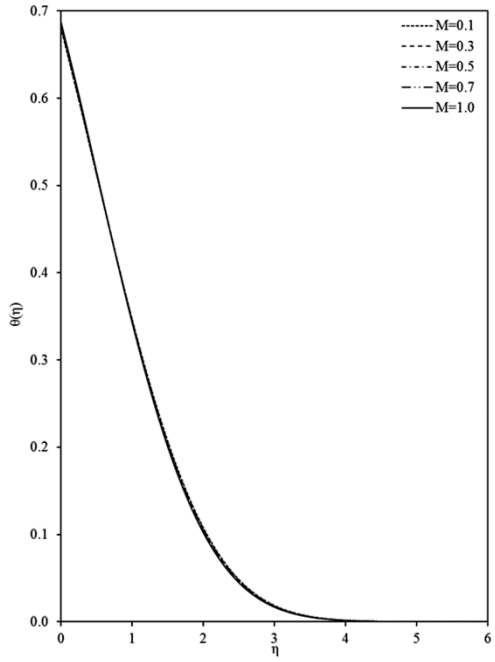

Fig. 7 – Temperature profiles of the CBC case for several values of M with $\varepsilon = 0.1$, $\gamma = 1.0$, $\Pr = 0.72$ and $Ec = 0.1$.

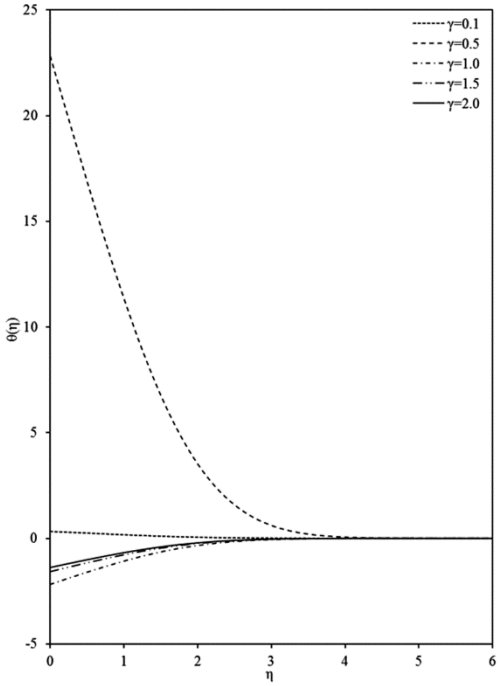

Fig. 8 – Temperature profiles of the NH case for several values of γ with $\varepsilon = 0.1$, $M = 0.1$, $\Pr = 0.72$ and $Ec = 0.1$.

CBC, it is appreciated that the thermal boundary layer thickness increases by increasing the conjugate parameter γ. This can be explained by the fact that the thermal resistance on the hot fluid side is proportional to heat transfer coefficient. Hence by

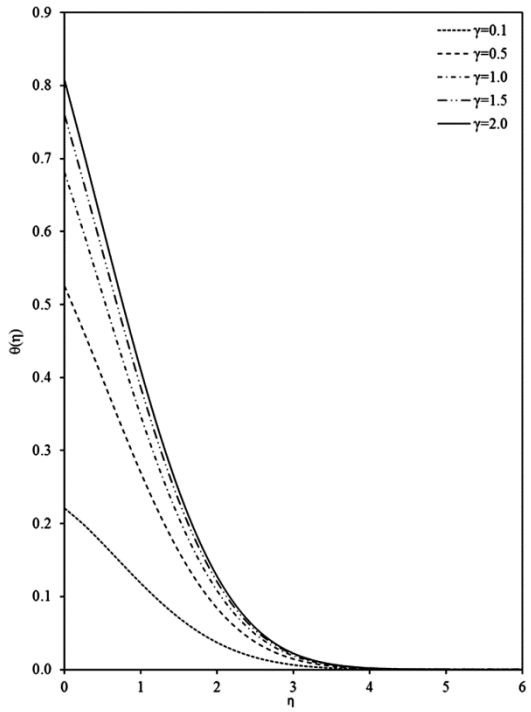

Fig. 9 – Temperature profiles of the CBC case for several values of γ with $\varepsilon = 0.1$, $M = 0.1$, $\Pr = 0.72$ and $Ec = 0.1$.

increasing amount in conjugate parameter, the hot fluid side convection decreases and as a result the surface temperature rises.

The impact of the Prandtl number $\Pr$ on the temperature field $\theta(\eta)$ is demonstrated in Figs 10 and 11 for the cases NH and CBC, respectively, taking other pertinent parameters constant. From these graphs, it is analyzed that the temperature decrease with increasing the Prandtl number $\Pr$, whereas in the case of NH reverse behavior is observed for $\eta > 1.5$. Therefore, an increase in the Prandtl number decreases the temperature as well as the thermal boundary layer thickness. On the other hand, it is noteworthy that the dimensionless temperature asymptotically approaches to zero in the free stream region. In this way, the Prandtl number governs the thermal boundary layers in heat transfer problems and can be adopted to raise the cooling rate.

Figures 12 and 13 examine the behaviors of the Eckert number Ec on the temperature $\theta(\eta)$ for the cases NH and CBC, respectively, while the other physical parameters are kept constant. An increase in the Eckert number Ec decreases the temperature for the case NH, which is opposite to the case CBC. These phenomenons occur because increasing the

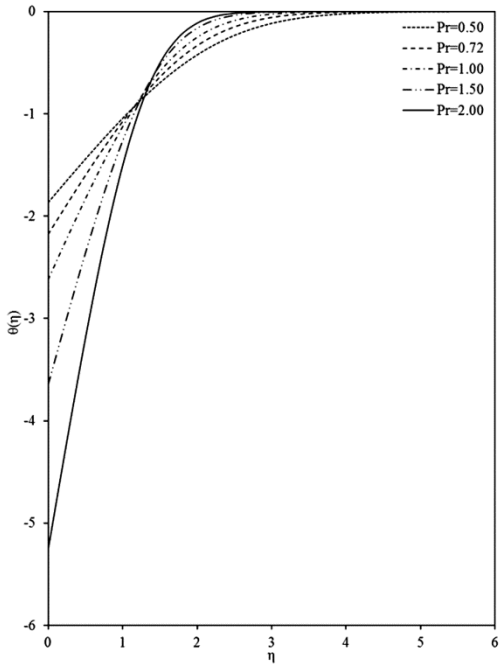

Fig. 10 – Temperature profiles of the NH case for several values of $\Pr$ with $\varepsilon = 0.1$, $M = 0.1$, $\gamma = 1.0$ and $Ec = 0.1$.

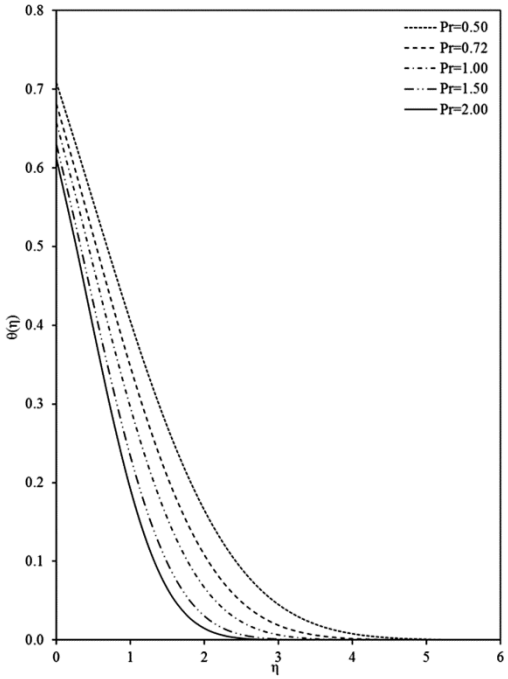

Fig. 11 – Temperature profiles of the CBC case for several values of $\Pr$ with $\varepsilon = 0.1$, $M = 0.1$, $\gamma = 1.0$ and $Ec = 0.1$.

values of the Eckert numbers generates heat in the fluid due to viscous dissipation. Ergo, viscous dissipation in a flow near the stagnation point is favorable for bringing up the temperature.

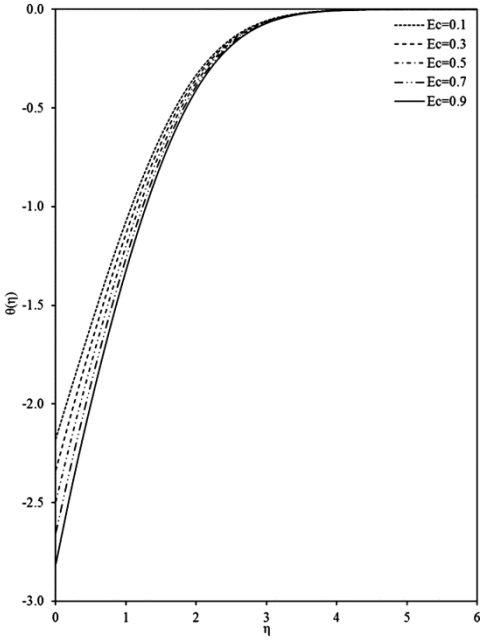

Fig. 12 – Temperature profiles of the NH case for several values of Ec with $\varepsilon = 0.1$, $M = 0.1$, $\gamma = 1.0$ and $\Pr = 0.72$.

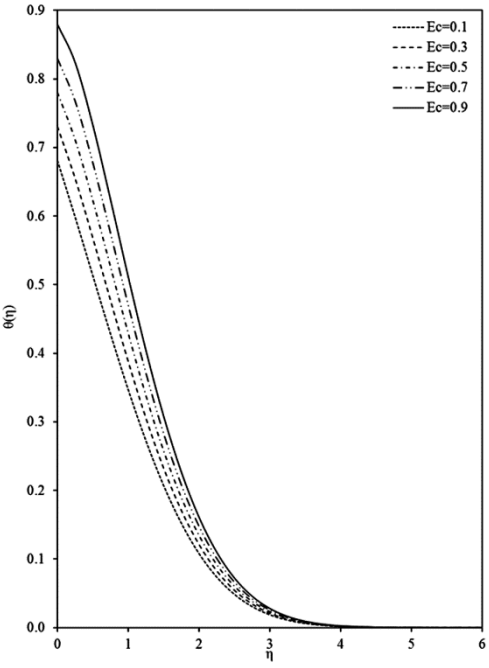

Fig.13 – Temperature profiles of the CBC case for several values of Ec with $\varepsilon = 0.1$, $M = 0.1$, $\gamma = 1.0$ and $\Pr = 0.72$.

Finally, Table 2 presents the effects of the stretching parameter ε, the magnetic parameter M, the conjugate parameter γ, the Prandtl number $\Pr$ and the Eckert number Ec on the wall shear stress $f''(0)$ and the heat transfer rate $\theta'(0)$ for all cases,

Table 2 – Numerical values of $f''(0)$ and $\theta'(0)$ for various values of physical parameters.

ε	M	γ	Pr	Ec	$f''(0)$	$\theta'(0)$ for NH	$-\theta'(0)$ for CBC
0.1	0.1	1.0	0.72	0.1	1.181020	1.178278	0.3188320
0.5					0.730376	1.508197	0.3655358
1.0					0.000000	2.096240	0.4037069
1.5					-0.887893	3.056350	0.4198880
2.0					-1.913175	4.797400	0.4140756
0.1	0.3				1.247159	1.206836	0.3172688
	0.5				1.310040	1.233507	0.3157446
	0.7				1.370097	1.258564	0.3142560
	1.0				1.4556254	1.293581	0.3120844
	0.1	0.1				-0.1325344	0.0779006
		0.5				-11.910250	0.2372890
		1.5				0.862380	0.3600787
		2.0				0.760442	0.3849807
		1.0	0.50			0.8671589	0.2917799
			1.00			1.621297	0.3425859
			1.50			2.649208	0.3702359
			2.00			4.261516	0.3881570
			0.72	0.3		1.336976	0.2692059
				0.5		1.495674	0.2195797
				0.7		1.654372	0.1699534
				0.9		1.813070	0.1203270

taking all other dimensionless parameters constant. Moreover $f''(0)$ and $\theta'(0)$ are proportional to the local skin friction C_f and the local Nusselt number Nu_x respectively. From the table, it is noted that an increase in the values of the stretching parameter ε leads to reduction in the wall shear stress $f''(0)$ while the opposite phenomenon occurs for the magnetic parameter M. Furthermore the positive values of wall shear stress for all values of the governing parameters are indicative of the physical fact that the fluid exerts a drag force on the surface. It is also clear that the heat transfer rate $\theta'(0)$ increases by increasing the stretching parameter ε, the magnetic parameter M, the Prandtl number Pr and the Eckert number Ec for all the cases but the reverse is true in case of CBC for the stretching parameter ε when $\varepsilon < 1.5$ and the Prandtl number Pr. Moreover, in all cases it is interesting to note that the local Nusselt number Nu_x is reduced with the rising values of the conjugate parameter γ but in the case NH, same nature is observed in reverse direction for $\gamma < 1$. From a physical point of view, positive sign of the heat transfer rate implies that there is a heat flow to the sheet and vice versa.

8 Conclusions

Numerical solutions have been obtained to study the stagnation point flow and heat transfer in a laminar flow of an incompressible, viscous and electrically conducting fluid past a stretching surface with Newtonian heating and convective boundary condition by considering viscous dissipation and Joule heating. The governing partial differential equations with the boundary conditions are converted to nonlinear ordinary differential equations by suitable similarity variables with appropriate boundary conditions. These equations are solved numerically by the Galerkin finite element method. From the results of the problem, the main findings can be summarized as follows:

(i) Momentum boundary layer thickness as well as surface heat flux in all cases raises with increasing values of the stretching parameter but reverse trend is observed in the CBC case for $\varepsilon < 1.5$. Consequently, thermal boundary layer thickness for all considered cases as well as shear stress reduces while the opposite is true for the NH case when $\eta > 2$.

(ii) An increase in the magnetic parameter leads to an increase in the fluid velocity, skin friction and Nusselt number in all analyzed cases. Subsequently fluid temperature for the NH case is reduced but is raised for $\eta > 1.5$. Furthermore reverse happens in the CBC case, as compared to the NH case.

(iii) For all reviewed cases, thickness of the thermal boundary layer increases and surface heat flux reduces with the increase of the conjugate parameter. When $\gamma < 1$, the nature of the flow has an inverted boundary layer structure in the NH case.

(iv) The effect of increasing value of the Prandtl number is to make the thermal boundary layer thin. While in the case of NH, the opposite phenomenon occurs for $\eta > 1.5$. On the other hand the heat transfer rate is increased in the NH case and decreased in the CBC case.

(v) In the presence of the increasing Eckert number, for the NH case, the thermal boundary layer becomes thinner and its skin friction increases. While in the case of CBC, temperature profiles as well as Nusselt number increases.

References

1 Rossow V J, *NACATN*, 1 (1957) 489.
2 Andersson H I, *Acta Mech*, 95 (1992) 227.
3 Ariel P D, *Acta Mech*, 105 (1994) 49.
4 Attia H A, *Appl Math Modell*, 26 (2002) 863.
5 Duwairi H M & Duwairi R M, *Heat Mass Trans*, 41 (2004) 51.
6 Xu H & Liao S J, *Meccanica*, 41 (2006) 599.
7 Chen T M, *J Thermophys Heat Trans*, 22 (2008) 125.
8 Fang T & Zhang J, *Commun Nonlinear Sci Numer Simul*, 14 (2009) 2853.
9 Jat R N & Chaudhary S, *ZAMP*, 61 (2010) 1151.
10 Guedda M & Ouahsine A, *Euro J Mech - B/Fluids*, 33 (2012) 87.
11 Chaudhary S & Kumar P, *Meccanica*, 49 (2014) 69.
12 Dogonchi A S, Divsalar K & Ganji D D, *Comput Meth Appl Mech Eng*, 310 (2016) 58.
13 Hiemenz K, *Dingler's Polytech J*, 326 (1911) 321.
14 Homann F, *ZAMP*, 16 (1936) 153.
15 Chiam T C, *J Phys Soc Jpn*, 63 (1994) 2443.
16 Lok Y Y, Phang P, Amin N & Pop I, *Int J Eng Sci*, 41 (2003) 173.
17 Reza M & Gupta A S, *Fluid Dyn Res*, 37 (2005) 334.
18 Nadeem S, Hussain M & Naz M, *Meccanica*, 45 (2010) 869.
19 Ja'fari M & Rahimi A B, *Scientia Iran*, 20 (2013) 152.
20 Chaudhary S & Choudhary M K, *Indian J Pure Appl Phys,* 54 (2016) 209.
21 Crane L J, *ZAMP,* 21 (1970) 645.
22 Siddappa B & Abel S, *ZAMP*, 36 (1985) 890.
23 Liao S, *Commun Nonlinear Sci Numer Simul*, 11 (2006) 326.
24 Makinde O D & Sibanda P, *Int J Numer Meth Heat Fluid Flow*, 21 (2011) 779.
25 Pal D, *Comput Math Appl*, 66 (2013) 1161.
26 Chaudhary S, Choudhary M K & Sharma R, *Meccanica*, 50 (2015) 1977.
27 Nield D A, *Trans Porous Med*, 75 (2008) 269.
28 Roy K & Murthy P V S N, *Int J Heat Mass Trans*, 91 (2015) 700.
29 El-Amin M F, *J Magn Magn Mater*, 263 (2003) 337.
30 Abo-Eldahab E M & El Aziz M A, *Appl Math Modell*, 29 (2005) 579.
31 Jat R N & Chaudhary S, *Il Nuovo Cimento B*, 124 (2009) 53.
32 Palani G & Kim K Y, *J Eng Thermophys*, 20 (2011) 501.
33 Chakraborty R, Dey R & Chakraborty S, *Int J Heat Mass Trans*, 67 (2013) 1151.
34 Hayat T, Imtiaz M & Alsaedi A, *Advance Powder Tech*, 27 (2016) 1301.
35 Merkin J H, *Int J Heat Fluid Flow*, 15 (1994) 392.
36 Lesnic D, Ingham D B, Pop I & Storr C, *Heat Mass Trans*, 40 (2004) 665.
37 Salleh M Z, Nazar R & Pop I, *J Taiwan Inst Chem Eng*, 41 (2010) 651.
38 Aydin O & Kaya A, *Heat Mass Trans*, 46 (2009) 129.
39 Yao S, Fang T & Zhong, Y, *Commun Nonlinear Sci Numer Simul*, 16 (2011) 752.
40 Nandy S K & Mahapatra T R, *Int J Heat Mass Trans*, 64 (2013) 1091.
41 Ibrahim W & Haq R U, *J Brazilian Soc Mech Sci Eng*, 38 (2016) 1155.
42 Mohamed M K A, Salleh M Z, Nazar R & Ishak A, *Bound Value Probl*, 2013 (2013) 4.
43 Wang C Y, *Int J Non-Linear Mech*, 43 (2008) 377.
44 Yacob N A & Ishak A, *Canadian J Chem Eng*, 90 (2012) 621.